Aflatoxin B1 detoxification by magnetic carbon nanostructures prepared from maize straw

Muhammad Zahoor[a],*, Farhat Ali Khan[a,b]

[a]*Department of Chemistry, University of Malakand, Chakdara Dir (Lower), Khyber Pakhtunkhwa, P.O. Box: 18000, Pakistan,*
Tel. +92945763441; Fax: +92945763491; emails: mohammadzahoorus@yahoo.com (M. Zahoor), farhatkhan2k9@yahoo.com
(F. Ali Khan)
[b]*Department of Pharmacy, Sarhad University of Science and Technology, Peshawar, Pakistan*

ABSTRACT

Magnetic carbon nanocomposites were prepared from maize wastes and were characterized by surface area analyzer, scanning electron microscopy (SEM), X-ray diffraction (XRD), Fourier transform infrared spectroscopy (FT-IR), thermogravimetric/differential thermal analysis (TG/DTA), and electron dispersive X-ray (EDX). The presence of iron oxide on the adsorbent surface was confirmed from SEM, XRD, and FT-IR analysis. Freundlich and Langmuir isotherms were used for the determination of adsorption parameters. The effect of pH on adsorption process was evaluated, and a decline in percent adsorption was noted at high pH. The equilibrium time at pH 7 and 3 was 96 and 180 min, respectively, and nearly 90% removal of aflatoxin B1 was achieved for both adsorbent. Pseudo-first-order and pseudo-second-order kinetic equations were used to analyze the kinetic data. Best fit was obtained with pseudo-first-order kinetics equation. The thermodynamics parameters were also determined, $\Delta S°$ was positive (64.438 kJ mol^{-1} deg^{-1}) while $\Delta H°$ (−16.24 kJ mol^{-1}) and $\Delta G°$ were negative (−1.949, −2.593, −3.238, and –3.882 kJ mol^{-1} corresponding to 30, 40, 50, and 60°C, respectively).

Keywords: Aflatoxins; Adsorption; Equilibrium time; Maize straw

1. Introduction

Aflatoxins are a major threat to poultry industry and human health. Aspergillus species especially *Aspergillus flavus* and *Aspergillus parasiticus* are mainly responsible for the production of aflatoxins [1]. Among aflatoxins, aflatoxin B1 ($C_{17}H_{12}O_6$) is of predominant importance. Contamination of aflatoxin B1 in poultry and animal feed stuffs presents the highest toxic potential due to teratogenicity, carcinogenicity, and mutagenicity [2,3]. Aflatoxins-contaminated feed is quite common in many countries and causes great economic losses to poultry industry in terms of growth retardation and high mortality rate. Moreover, accumulation of aflatoxin in different tissues of poultry may indirectly result in health risk to human [4].

Prevention of aflatoxin contamination in feed is very important, but when contamination occurs, decontamination of feed is needed before using it. Feasibly, large scale production and economically efficient methods for remediation of aflatoxins in feeds is need of the day [1]. A number of biological, chemical,

*Corresponding author.

and physical treatments are utilized for detoxification of aflatoxin-contaminated feed and feed stuffs. Most of these methods are costly, time consuming, and less effective [5,6]. The most practical approach for detoxifying aflatoxins in poultry feed is the use of adsorbent [7,8]. Adsorbent binds aflatoxins and inhibits their absorption from gastrointestinal tract [9]. Most of the adsorbents have established effectiveness, but their large quantities and negative interaction with nutrients with feed are causes of great concern. The activated carbon although is excellent adsorbent for organic and inorganic pollutants. However it causes dehydration and salt deficiencies when administered to poultry birds [10,11].

There is considerable focus on magnetic particle technology due to its application in environmental problems. Adsorption of contaminants from aqueous or gaseous effluents through magnetic adsorbents is largely employed these days. Such adsorbents can be removed from media by the use of magnetic field after use. Relatively small surface area and less adsorption capacity are the discredits of these materials that shorten their use [12]. Moreover their preparation requires several steps and special chemical procedures. The activated carbon is being used as a gorgeous and cheap source for the adsorption of organic and inorganic pollutants. By virtue of its high surface area and porous structure it can remove organic compounds dispersed or dissolved in liquids [13]. In addition, the small particle size of iron oxide produced on the surface of carbon allows rapid adsorption. According to Kahani et al., the conversion of biomass into magnetic carbon nanocomposites would provide an excellent and cheap adsorbent for the remediation environmental problems [13]. In this research work, a new, simple, and cost-effective method was applied for the preparation of magnetic carbon nanocomposites from maize straw as aflatoxin B1 binder. The equilibrium data, kinetics, effect of pH, and temperature were investigated to know its adsorption mechanism.

2. Experimental

2.1. Samples preparation and characterization

In this work, the maize straw was used as biomass for the preparation of magnetic carbon nanocomposites. The biomass was converted into small pieces and transferred to ethanolic $FeCl_3 \cdot 6H_2O$ (1 g/10 ml). After 30 min, the biomass were separated through filtration and dried under air current for 24 h. Then, the biomass was ignited in nitrogen atmosphere in a specially designed chamber (designed by the author) consisting of a stainless steel container equipped with an electric
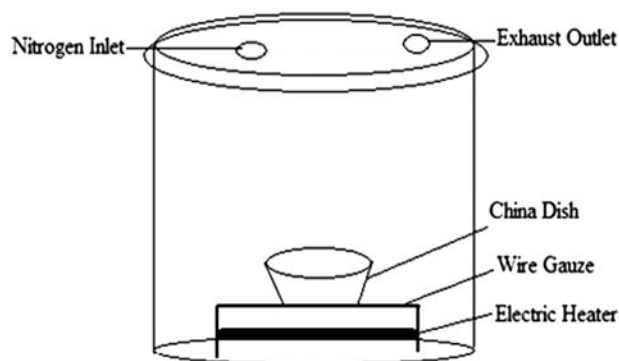

Fig. 1. Diagram of the chamber used for the preparation of adsorbent.

heater, wire gauze, nitrogen gas inlet, and exhaust outlet (Fig. 1). During heating, the iron chloride converted to Fe_3O_4 leads to the development of magnetic character in the prepared adsorbent. The prepared adsorbent was characterized by surface area analyzer (Quantachrome instrument v2.1), Joel X-ray diffractometer JDX-3532 with Ni filter, using monochromatic CuKa radiation of wave length 1.5418A°. The X-ray generator was operated at 40 KV and 30 mA. The scanning range $2\theta/\theta$ was selected. The scanning speed 10 min^{-1} was employed for precise determination. Infrared spectra were collected by using Fourier transform infrared spectrometer (IR Prestige fourier transform infrared spectrophotometer, Shimadzo, Japan) ranging 750–525 cm^{-1} and 4,000–600 cm^{-1}. The surface morphology of the sample was examined using Joel jsm-5910 type scanning electron microscope (SEM) at an accelerating voltage of 20 KV. The energy dispersive X-ray analysis was performed by using EDS X-sight oxford instrument, while the differential thermal analysis (DTA) and thermal gravimetric analysis were done using Diamond Series TG/DTA Perkin Elmer, USA analyzer using Al_2O_3 as reference.

2.2. Determination of kinetics parameters

The analysis of aflatoxin B1 was carried out by reported method of Stroka et al. [14]. A series of 25 ml flasks were taken and added 5.4 ml ethanol and 13 ml distilled water (pH 3 or 7). Sample of sorbent 0.5% was transferred to each flask and spiked with known amount of standard aflatoxin B1 to make the required level (200 ppm). All the flasks were then kept on rotary shaker with a speed of 300 rpm at room temperature. The sorbent was separated from each flask at different time interval through magnetic bar. The contents in the flasks were then filtered through Whatman paper No. 1 and analyzed by HPLC.

The HPLC system consisted of Hitachi model L-200 equipped with two pumps L-2130, auto injector L-2200 and fluorescence detector L-2458 (Macoa, Japan) was used for aflatoxin B1 analysis.

2.3. LC analysis

Degassing of the mobile phase acetonitrile/methanol/water (8:27:65, v/v/v) was done by sonication. The column intersil ODS-3 (25 cm × 4.5 mm I.D., 5 μm, GL science, Tokyo, Japan) was connected to LC column. The column was maintained at 40°C with a flow rate of 0.8 ml/min, while the injection volume was 20 μl. The aflatoxin B1 was detected at the excitation and emission wavelengths of 365 and 450 nm, respectively. For quantification, a separate calibration curve was established. Triplicate samples were used for setting the calibration curve, determining limit of detections (LODs), and extraction recovery. Limit of detections (LODs) and limit of quantification (LOQ) were determined by diluting the standard solution of known concentration at sound to noise ratio of 3 and 10 respectively (Fig. 2).

2.4. Determination of adsorption parameters

To a series of 25 ml-flasks (1–15) containing 5.4 ml ethanol and 13 ml distilled water, added 0.5% sorbent and spiked with known amounts of aflatoxin B1 standard to achieve the desired levels (150, 175, 200, 225, 250, 275, 300, 325, and 350 ppm). The amount of aflatoxin B1 adsorbed by flasks was inappreciable up to 13 h. All the flasks were placed on rotary shaker with a 300 rpm for 480 min at room temperature. The sorbents were then separated by magnetic bar from each flask, while the contents in the flasks were filtered through Whatman paper No. 1 and analyzed using HPLC as discussed above.

2.5. Determination of effect of pH on adsorption of aflatoxin B1

To a series of 25 ml-flasks (1–14) containing 5.4 ml ethanol and 13 ml distilled water (pH 1–14), added 0.5% sorbents. Each flask was spiked with standard aflatoxin B1 to achieve the concentration of 200 ppm. All the flasks were kept on rotary shaker with a speed of 300 rpm for 240 min. The sorbent was then separated from the solution by magnetic bar, while the content in the flasks was filtered through Whatman paper No. 1 and subjected to HPLC for aflatoxin B1 analysis as mentioned above.

2.6. Determination thermodynamics parameters

Sorbent of 0.5% was added to 5.4 ml ethanol and 13 ml of distilled water in conical flasks. All the flasks were spiked by standard aflatoxin B1 to achieve the desired concentration (200 ppm) and placed on shaker incubators with a speed of 300 rpm at 30, 40, 50, and 60°C each. The sorbent was then separated from the solution using magnetic bar, filtered the solution through Whatman paper No. 1 and analyzed for aflatoxin B1 by HPLC as discussed above.

3. Results and discussion

3.1. Characterization of the nanostructures

The composites were prepared on a carbon surface. After preparation, magnetic bar was applied to the material which completely attached to the magnet. This showed that the whole material was magnetite.
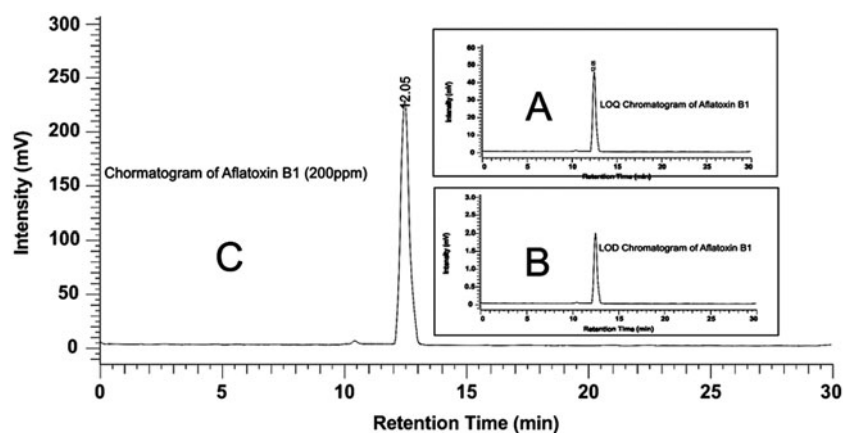

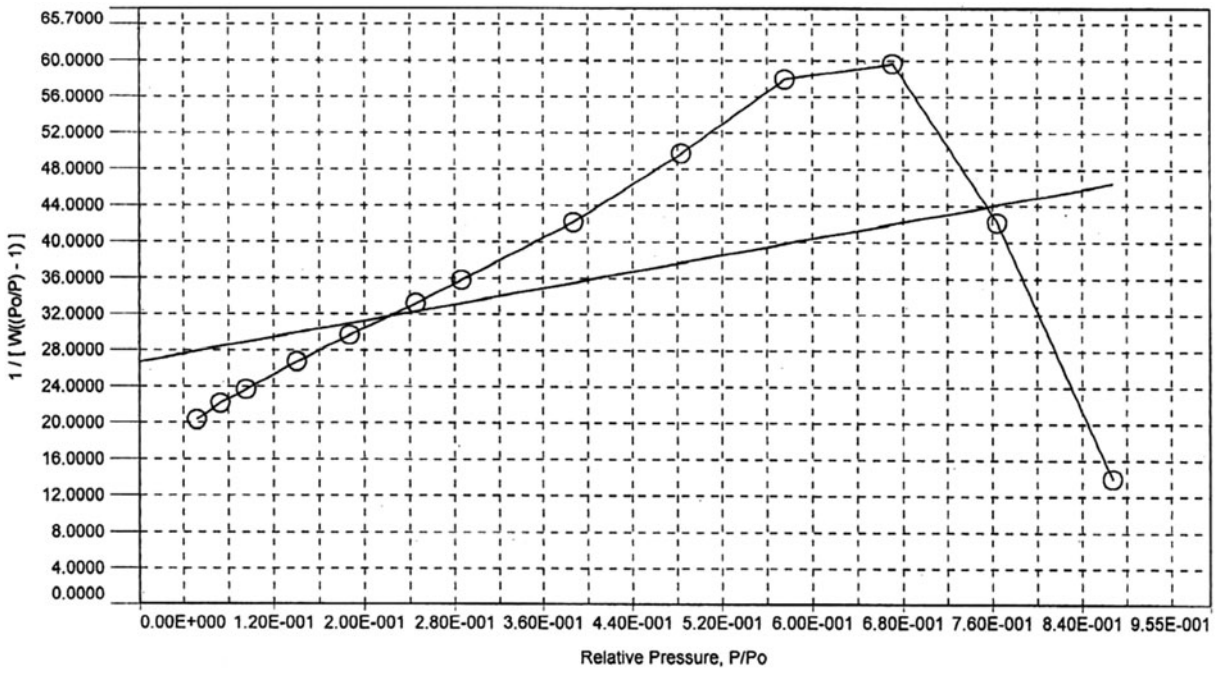Fig. 2. HPLC Chromatogram of aflatoxin B1 at LOD and LOQ.

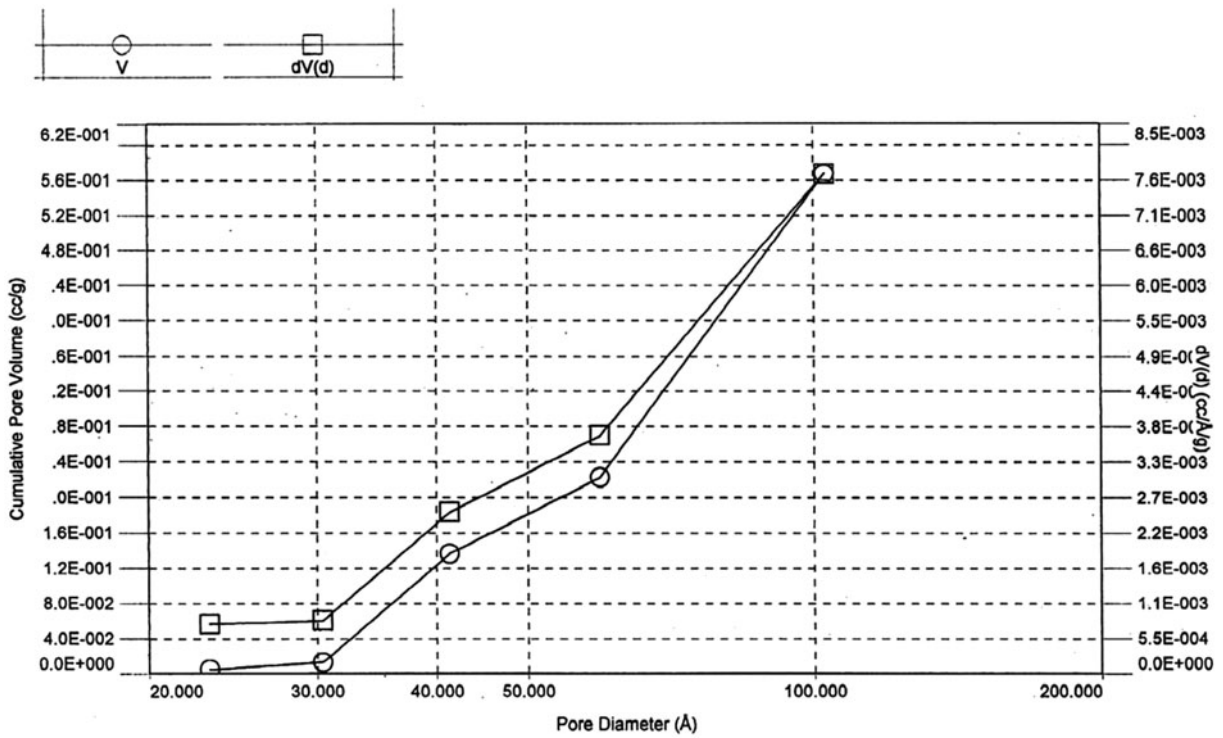Fig. 3(a). Graphical representation of BET surface area of the prepared adsorbent.

Fig. 3(b). Graphical representation of pores distribution in the prepared adsorbent.

The surface area of the prepared adsorbent is shown in Fig. 3(a) while pores distribution is given in Fig. 3(b). The different surface parameters are shown in Table 1.

X-ray diffraction (XRD) method is not only used for structure determination but to the particles size measurement [15]. XRD analysis of magnetic carbon nanocomposites is shown in Fig. 4 which suggested the presence of Fe_3O_4 deposited in the carbon. The diffraction peaks at 2θ of 30.1, 35.8, 44.45, 54.2, 57.95, and 62.55 represents the corresponding indices (2 2 0), (3 1 1), (4 0 0), (4 2 2), (5 1 1), and (4 4 0) planes of cubic unite cell, which correspond to the magnetite structure previously reported by [16,17]. The diffraction peaks at 2θ of 24.3, 33.3, 41, 48.6, 49.6, and 60.15 may be related to the presence of maghemite and some hematite matches the results of [16]. The magnetic carbon nanocomposites size was obtained using Debye–Scherer's equation

$$D = K\lambda/\beta \, \mathrm{Cos} \, \theta \tag{1}$$

where D is the mean size, K is the constant (0.94), λ is the wavelength (1.54060 A˚) of X-ray, β is the excess line broadening, and θ is the Bragg angle.

$$\beta = B - b \tag{2}$$

Table 1
Physical parameters of the prepared adsorbent

BET surface area (m^2/g)	70.50
Langmuir surface area (m^2/g)	254.90
Total pores volume (cm^3/g)	0.57
Micropores volume (cm^3/g)	0.29
Average pore diameter (Å)	102.86

where B stands for line width (radian) and b is instrument line broadening (radian) [18]. By using the formula, the composite sizes were found to be in the range of 80–300 nm.

Infrared spectroscopy is the most widely used techniques for iron oxide characterization. It is a useful technique to show information about crystal morphology, nature of surface hydroxyl groups, and adsorbed H_2O. Usually in literature, the broad band at 580 and 400 cm^{-1} corresponds to various magnetite samples [13]. The IR spectrums (far and mid regions Figs. 5(a) and 5(b)) of magnetic carbon nanocomposites show broad band at 1,039.63 and 574.79 cm^{-1}. The intense peak in the regions of 1,000–1,200 correspond to stretching of C–C and C–O in carbon [13], and 574.70 can be attributed to stretching of Fe–O deposited magnetite.

The morphology of magnetic carbon nanocomposites is shown in Fig. 6 with low and high magnification. SEM observation showed some differences in size and shape of the composites. The white patches in the images show the crystallization of the sample, while the black portions represent the carbon. SEM monograph also reveals aggregation of particles which is due to the moisture contents absorbed in the sample. The aggregation of particles decreases the surface area of adsorbent and thus decreases its adsorption capacity. It was also observed from the images that the shape of the Fe_3O_4 appears somewhat cubical.

The two dehydration stages are shown by Thermogravimetric analysis curves (Fig. 7). About 11% of mass loss was observed, and this mass loss is mainly in the temperature range from 40˚—230˚C, and a very small mass loss was noted when heated to

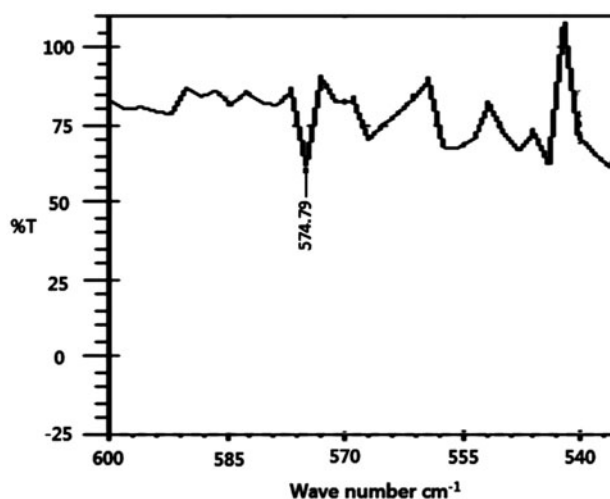Fig. 4. XRD pattern of magnetic carbon nanocomposites.

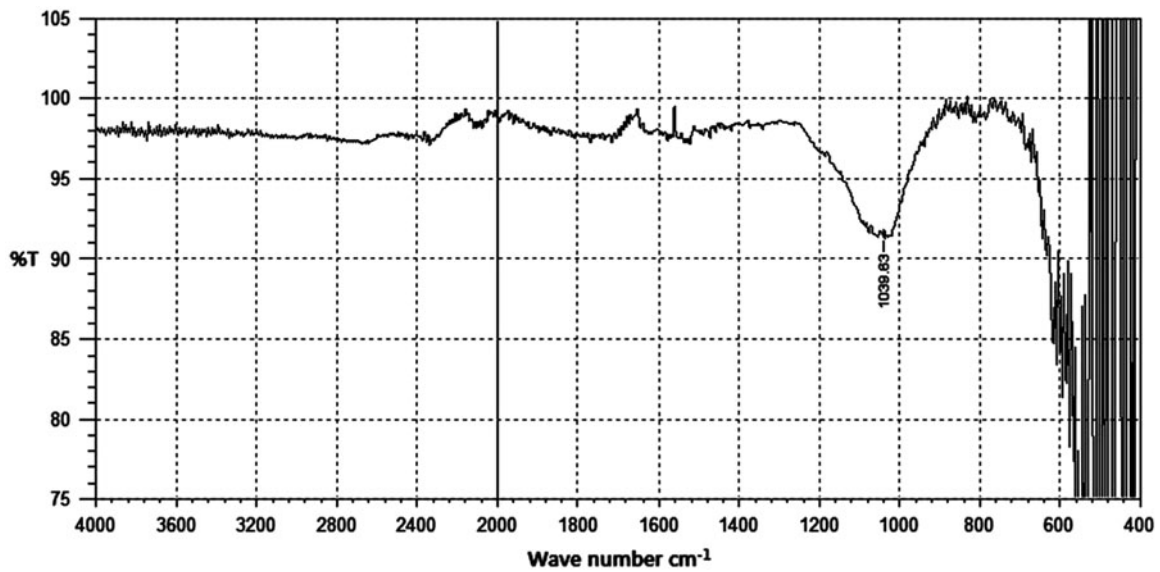Fig. 5(a). Far IR of magnetic carbon nanocomposites.

Fig. 5(b). Mid IR of magnetic carbon nanocomposites.
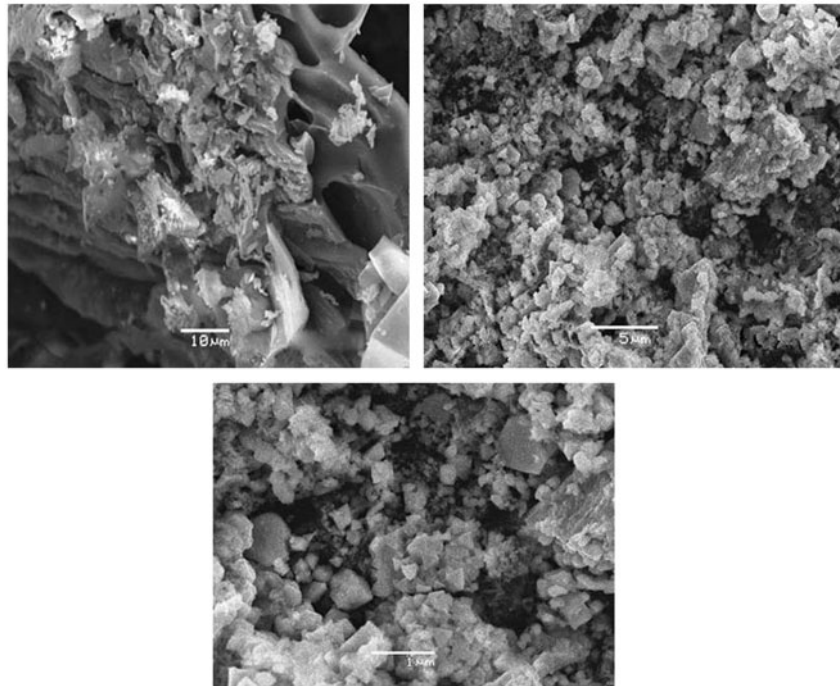

Fig. 6. SEM images of magnetic carbon nanocomposites at different magnification.

600°C. Observed loss of mass is due to the loss of water of hydration of Fe_3O_4 nanocomposites. DTA curves show two endothermic peaks in the temperature range 25°C—250°C.

Electron dispersive X-ray (EDX) analysis of magnetic carbon nanocomposites is shown in Fig. 8 which

reveals the presence of iron (Fe), oxygen (O), and carbon (C). While a small peak representing Calcium (Ca) as an impurity was also observed. In magnetic carbon nanocomposites, O-Kα, Fe-Lα, Fe-Kα, and Fe-Kβ peaks show the presence of magnetite deposition which is in conformity to [13].
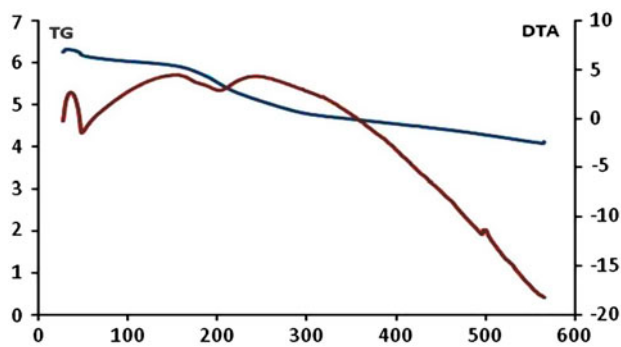
Fig. 7. TG/DTA curves of magnetic carbon nanocomposites.

Fig. 9. Giles isotherm for the adsorption of aflatoxin B1 on carbon nanocomposites.

substrate bonds and more solute molecules inter into sites not penetrated by solvent.

The adsorption of aflatoxin on the prepared adsorbent was quantified by using Langmuir [20] and Freundlich [21] adsorption isotherms. Giles isotherms are used to determine the behavior of adsorbate adsorption on adsorbent while Langmuir and Freundlich adsorption isotherms are used for quantitative purposes. Langmuir adsorption isotherm is based on the assumption that the maximum adsorption corresponds to a saturated monolayer of solute molecules on the adsorbent surface, with no interaction from lateral sides adsorbed molecules. The linearized form of Langmuir isotherm is given as:

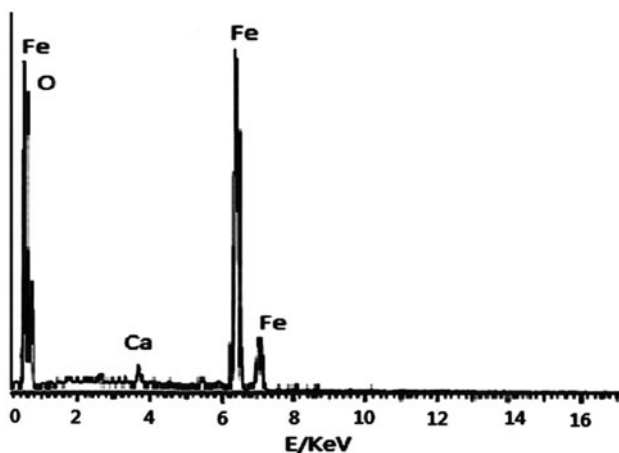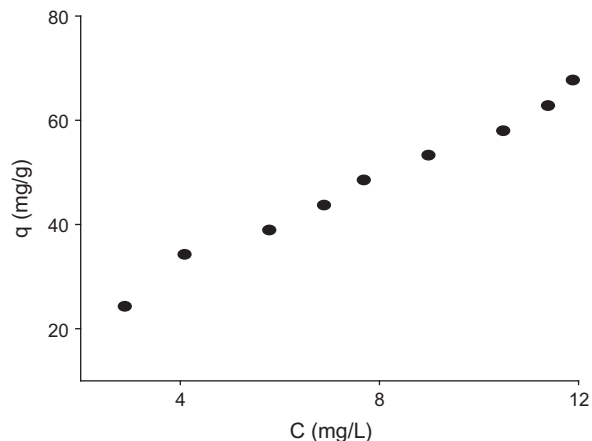$$\frac{C}{q} = \frac{C}{Q_0} - \frac{1}{Q_0 b} \tag{3}$$

Fig. 8. EDX spectra of magnetic carbon nanocomposites.

3.2. Adsorption isotherm

The adsorption of aflatoxin B1on the prepared adsorbent was studied. Giles adsorption isotherm [19] was obtained by plotting C (concentration) vs. q (amount of aflatoxin adsorbed). The Giles adsorption isotherm is shown in Fig. 8. Based on their initial slope and curvature, Giles classified the isotherms into constant partition C, high affinity H, Langmuir L, and sigmoidal-shaped S-type. The isotherm in Fig. 9 is C-type. In this type of curves, the availability of adsorption sites remains constant at all concentrations up to saturation. It is characterized by the constant partition of contaminant between solution and substrate up to maximum possible adsorption. The linearity of the curve indicates that the number of adsorption sites remains constant and, as adsorption promotes, more and more sites are created. This situation arises when there is strong attraction of solute for adsorbent than solvent. The solute then breaks inters
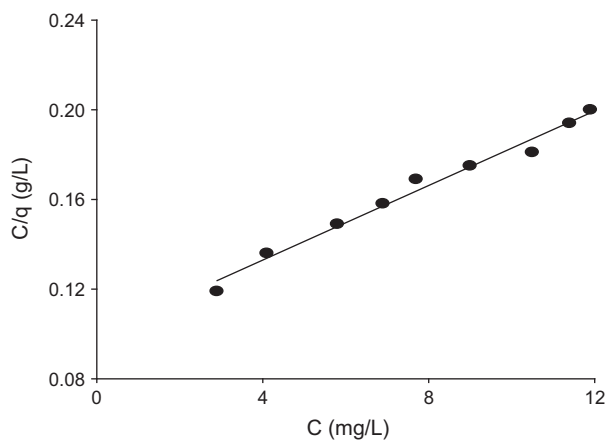

Fig. 10. Langmuir plot for the adsorption of aflatoxin B1 on carbon nanocomposites.

Table 2
Isotherm parameters for the adsorption of aflatoxin B1 on carbon nanocomposites

Substance	Langmuir isotherm			Freundlich isotherm		
	Q_0 (mg g^{-1})	b (L mg^{-1})	R^2	K (mg g^{-1}(L mg^{-1})$^{1/n}$)	$1/n$	R^2
Aflatoxin B1	120.28	0.0834	0.983	31.13	0.677	0.987

where q is the amount of aflatoxin adsorbed in mg g^{-1}, C is the equilibrium concentration of aflatoxin in mg L^{-1}, Q_0 and b are Langmuir constants. Q_0 is the maximum adsorption capacity of the adsorbent while b is the energy of the process. The plot of specific adsorption (C/q) against equilibrium concentration is shown in Fig. 10, and the Langmuir constants Q_0 and b were calculated from the slope and intercept of the plot are given in Table 2.

The Freundlich isotherm is usually used to describe heterogeneous systems. The Freundlich isotherm is represented by following equation.

$$\ln q = \ln K + \frac{1}{n}\ln C \qquad (4)$$

where C represents the equilibrium concentration in mg L^{-1}, q is the amount of aflatoxin adsorbed in mg g^{-1}, K and n are Freundlich constants. K represents adsorption capacity while n represents the adsorption intensity. The values of these constants were calculated from the slope and the intercept of the ln C vs. ln q plot (Fig. 11) and are given in Table 2.

3.3. Adsorption kinetics

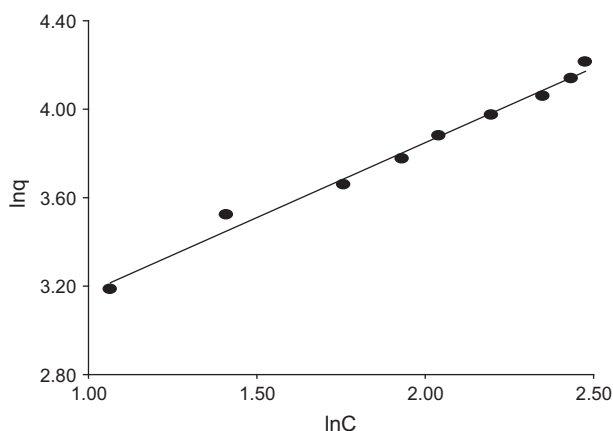The time of contact required to reach equilibrium for an adsorbent is an important factor in adsorption processes. Time t verses C plot for 200 ppm, and aflatoxin solutions at pH 3 and 7 are shown in Fig. 12. The fast uptake of aflatoxin occurs within the first few minutes as initially the adsorbents sites are free and more available for the adsorption of aflatoxin. With passage of time, as more and more sites are occupied, the adsorption process become slow. Finally, a saturation point is reached that corresponds to the equilibrium time of adsorption. The equilibrium time for the adsorption of aflatoxin 200 ppm at pH 7 and 3 are 96 and 180 min, respectively. At equilibrium, nearly 90% removal of aflatoxin B1 was achieved for both adsorbents. The longer equilibrium time at pH 3 was due to the fact that iron oxide present in the structure of the composite dissolved in acidic media and results in generation of new micropores that needs longer time to saturate, while at pH, the iron oxide remain intact in the composite structure [22]. The reason for carrying out the experiments at pH 3 and 7 is that the adsorbent will be tested in the in vivo study at stomach and intestine pH.

Pseudo-first-order [23] and pseudo-second-order [24] adsorption kinetics equations were used to analyze the adsorption kinetics data. The pseudo-first-order equation is given as:

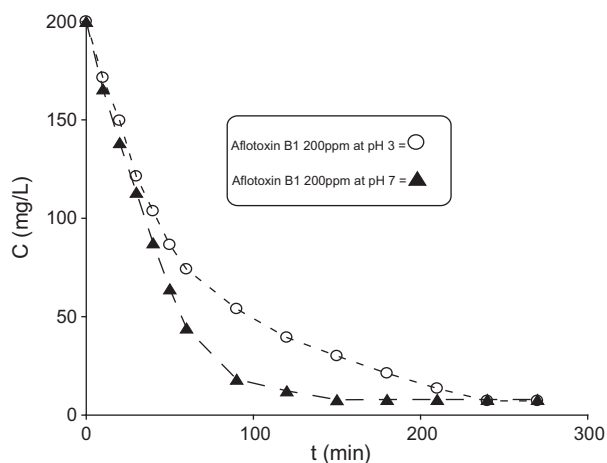$$\ln(q_e - q) = \ln q_e - k_a t \qquad (5)$$

Fig. 11. Freundlich plot for the adsorption of aflatoxin B1 on carbon nanocomposites.

Fig. 12. Effect of contact time of aflatoxin B1 adsorption on carbon nanocomposites.

where q_e is the amount of aflatoxin sorbed in mg g^{-1} at equilibrium while q is its amount adsorbed in mg g^{-1} at time t and k_a (min^{-1}) is the first order rate constant. This equation shows a linear relationship between ln (q_e-q) and t. The plot of ln (q_e-q) vs. t is shown in Fig. 13. The values of k_a and R^2 are given in Table 3.

The pseudo-second-order kinetics equation is given as follow.

$$\frac{t}{q_t} = \frac{1}{K_2 q^2} + \left(\frac{1}{q}\right)t \qquad (6)$$

By plotting t/q vs. t, a straight line was obtained, and the values of K_2 and q were calculated from intercepts and slopes of the plot as shown in Fig. 14. The values of K_2 and R_2 for the prepared adsorbent are given in Table 3.

Table 3 shows that the adsorption kinetics of aflatoxin at two different pH and same agitation speed could be best explained in terms of the pseudo-first-order rate equation with precision in the correlation coefficients, while pseudo-second-order rate equation did not reflect the experimental results.
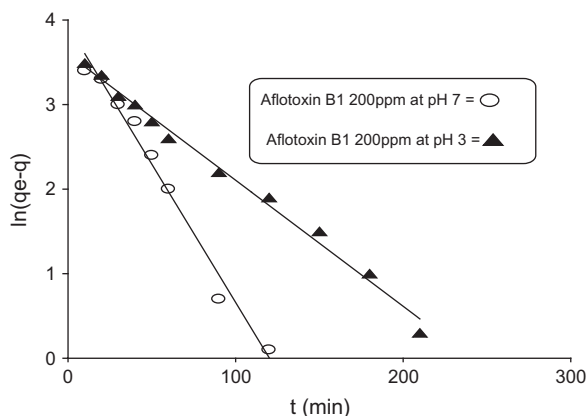
3.4. Effect of pH

pH is an important factor that affects the adsorption process by affecting the surface charge of the adsorbent and the degree of ionization and speciation of the adsorbate. The effect of pH on aflatoxin adsorption is shown in Fig. 15. The figure shows that the amount of aflatoxin adsorbed is not much affected from pH 1 to pH 11; however, above this, the decline was observed. This could be explained by the fact that iron oxide is highly soluble in acidic medium as compared to alkaline, thus creating new pores in the carbon composite for adsorb maximum aflatoxin B1.

3.5. Adsorption thermodynamics

To determine the adsorption thermodynamics, the adsorption experiment was carried out at 30, 40, 50, and 60℃. The Van't Hoff equation is used to determine $\Delta H°$ and $\Delta S°$ of the adsorption process.

$$\ln K = \frac{\Delta S°}{R} - \frac{\Delta H°}{RT} \qquad (7)$$

Fig. 13. Pseudo-first-order kinetics plots for the adsorption of aflatoxin B1 on carbon nanocomposites.
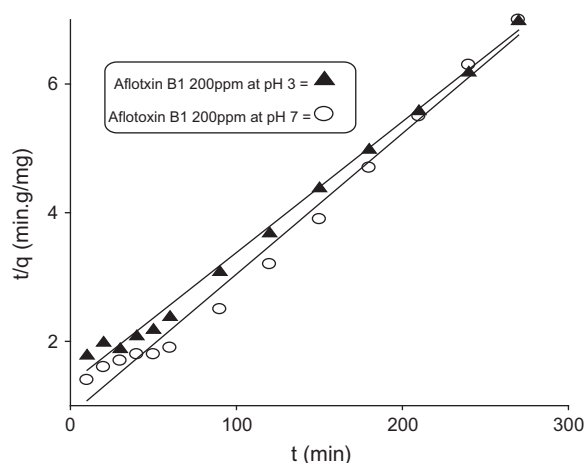

Fig. 14. Pseudo-second-order kinetics plots for the adsorption of aflatoxin B1 on carbon nanocomposites.

Table 3
Pseudo-first-order and pseudo-second-order adsorption rate constants and correlation coefficients for the adsorption of aflatoxin of carbon nanocomposites

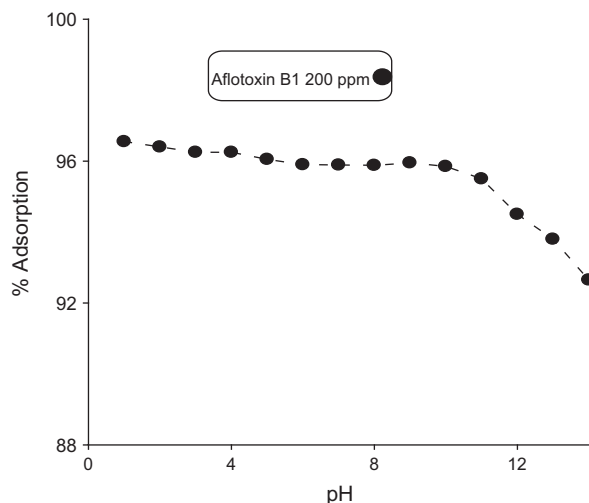| Substance	Concentration (ppm)	pH	Pseudo-first-order kinetics model		Pseudo-second-order kinetics model	
			k_a	R^2	K_2	R^2
Aflatoxin B1	200	3	0.015	0.99	0.0038	0.82
Aflatoxin B1	200	7	0.033	0.98	0.0023	0.65

Fig. 15. Effect of pH on adsorption of aflatoxin B1 by carbon nanocomposites.

K is the distribution constant of adsorption, $\Delta H°$ is the enthalpy change, $\Delta S°$ is the entropy change and T is the temperature in kelvin while R is universal gas constant. The value of $\Delta H°$ was calculated from the slope while $\Delta S°$ was calculated from intercept of the $\ln K$ and $1/T$ plot (Fig. 16) and found to be -16.24 and 64.438 kJ mol^{-1} deg^{-1}, respectively. The positive value of $\Delta S°$ shows that there is an increase in the randomness in the system solid/solution interface during the adsorption process, while the negative value of $\Delta H°$ shows that the adsorption of aflatoxin on the prepared carbon nanocomposites is an exothermic process.
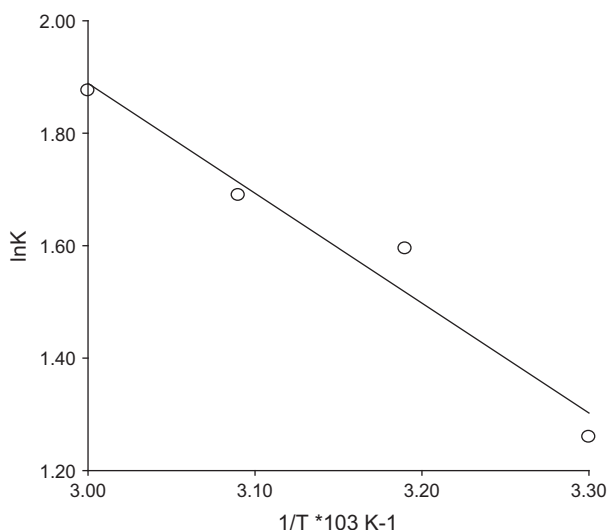
The values of standard free energy $\Delta G°$ were calculated from equation:

$$\Delta G° = \Delta H° - T\Delta S° \tag{8}$$

The values calculated from equation, -1.949, -2.593, -3.238, and -3.882 kJ mol^{-1} corresponds to 30, 40, 50, and 60℃, respectively. The negative values of $\Delta G°$ at various temperatures specify the spontaneous nature of the process and a high affinity of aflatoxin for the prepared adsorbent. The increase in $\Delta G°$ with the rise in temperature indicates that the process of adsorption is more favorable at high temperatures.

4. Conclusions

The prepared adsorbent was used for the removal of aflatoxin B1. The equilibrium time was 96 min for 200 ppm at pH 3 while 180 min at pH 7 where nearly 90% of aflatoxin was removed from solution at equilibrium, while best fit was obtained with pseudo-first-order kinetics model. At pH value above 11, there was a decline in percent adsorption. $\Delta S°$ value was positive while that of $\Delta H°$ and $\Delta G°$ were negative. At high temperature (60℃), $\Delta G°$ value was high as compared that of at 30℃ which shows that the adsorption process is favorable at high temperature. Thus, the prepared magnetic adsorbent can be used as alternative of activated carbon for the detoxification of aflatoxin in poultry feed as the former cause dehydration and salt deficiencies when given to poultry birds. In our *in vivo*, the adsorbent will be tested for the purpose mentioned.

Fig. 16. Van't Hoff plot for the adsorption of aflatoxin B1 on carbon nanocomposites.

References

[1] H. Basmacıoglu, H. Oguz, M. Ergull, R. Col, Y.O. Birdane, Effect of dietary esterified glucomannanon performance, serum biochemistry and haematologyin broilers exposed to aflatoxin, Czech J. Anim. Sci. 50 (2005) 31–39.

[2] M. Ortatatli, H. Oğuz, Ameliorative effects of dietary clinoptilolite on pathological changes in broiler chickens during aflatoxicosis, Res. Vet. Sci. 71 (2001) 59–66.

[3] E. Sur, İ. Celİk, Effects of aflatoxin B 1 on the development of the bursa of Fabricius and blood lymphocyte acid phosphatase of the chicken, Br. Poultry Sci. 44 (2003) 558–566.

[4] B.M. Bhatti, T. Talat, R. Sardar, Estimation of aflatoxin B1 in feed ingredients and compound poultry feeds, Pak. Vet. J. 21 (2001) 57–60.

[5] CAST (Council for Agricultural Science and Technology), Task Force Report 16. Mycotoxins: Economic and Health Risks, CAST, Ames, IA, 1989.

[6] K.S. McKenzie, A.B. Sarr, K. Mayura, R.H. Bailey, D.R. Miller, T.D. Rogers, W.P. Norred, K.A. Voss, R.D. Plattner, L.F. Kubena, T.D. Phillips, Oxidative degradation and detoxification of mycotoxins using a novel source of ozone, Food Chem. Toxicol. 35 (1997) 807–820.

[7] A. Huwig, S. Freimund, O. Käppeli, H. Dutler, Mycotoxin detoxication of animal feed by different adsorbents, Toxicol. Lett. 122 (2001) 179–188.

[8] M. Peraica, A. Domijan, Z. Jurjevic, B. Cvjetkovic, Prevention of exposure to mycotoxins from food and feed, Arch. Hig. Rada. Toksikol. 53 (2002) 229–237.

[9] I. Kannewischer, M.T. Arvide, G.N. White, J.B. Dixon, Smectite clays as adsorbents of aflatoxin B1: Initial steps, Clay Sci. 2 (2006) 199–204.

[10] R. Miazzo, C.A. Rosa, E.C. De Queiroz Carvalho, C. Magnoli, S.M. Chiacchiera, G. Palacio, M. Saenz, A. Kikot, E. Basaldella, A. Dalcero, Efficacy of synthetic zeolite to reduce the toxicity of aflatoxin in broiler chicks, Poultr. Sci. 79 (2000) 1–6.

[11] C.A. Rosa, R. Miazzo, C. Magnoli, M. Salvano, S.M. Chiacchiera, S. Ferrero, M. Saenz, E.C. Carvalho, A. Dalcero, Evaluation of the efficacy of bentonite from the south of Argentina to ameliorate the toxic effects of aflatoxin in broilers, Poultry Sci. 80 (2001) 139–144.

[12] L.C.A. Oliveira, R.A. Rios, J.D. Fabris, V. Garg, K. Sapag, R.M. Lago, Activated carbon/iron oxide magnetic composites for adsorption of contaminants in water, Carbon 40 (2000) 2177–2183.

[13] S.A. Kahani, M. Hamadanian, O. Vandadi, Deposition of magnetite nanoparticles in activated carbons and preparation of magnetic activated carbons. Nanotechnology and its applications, First Sharjah International Conference, American Institute of Physics, 2007.

[14] J. Stroka, E. Ankalam, U. Jorissen, J. Gilbert, Immunoafinity column cleanup with liquid chromatography using post-column bromination for determination of aflatoxins in peanut butter, pistachio paste, fig paste, paprika powder. Collaborative study, J. Assoc. Anal. Chem. Inter. 83 (2000) 320–340.

[15] B.D. Cullity, Element of X-ray Diffraction, Addison Wesley, Reading, MA, 1974.

[16] S. Krehula, S. Music, Formation of magnetite in highly alkaline media in the presence of small amounts of ruthenium, Croat. Chem. Acta CCACAA 80 (2007) 517–527.

[17] X. Liu, Jang-Kyo Kim, Solvothermal synthesis and magnetic properties of magnetite nanoplatelets, Mater. Lett. 63 (2009) 428–430.

[18] M. Sundrarajan, M. Ramalakshmi, Novel cubic magnetite nanoparticle synthesis using room temperature ionic liquid, E.-J. Chem. 9 (2012) 1070–1076.

[19] C.H. Giles, T.H. Macewan, S.N. Nakhwa, D. Smith, Studies in adsorption. Part IX. A system of classification of solution adsorption isotherms and its use in diagnosis of adsorption mechanisims and in measurement of specific surface areas of solids, J. Chem. Soc. 30 (1960) 3973–3993.

[20] I. Langmuir, The adsorption of gases on plane surfaces of glass, mica and platinum, J. Am. Chem. Soc. 40 (1918) 1361–1403.

[21] H. Freundlich, Uber die adsorption in losungen (Adsorption in solution), Z. Phys. Chem. 57 (1906) 384–470.

[22] C. Wang, D. Ma, X. Bao, Transformation of biomass into porous graphitic carbon nanostructures by microwave irradiation, J. Phys. Chem. C 112 (2008) 17596–17602.

[23] S. Lagergren, Zurtheorie der sogenannten adsorption geloesterstoffe (About the theory of so-called adsorption of soluble substances), Kungliga Svenska Vetenskapsakademiens, Handlingar 24 (1898) 1–39.

[24] Y.S. Ho, G. McKay, Sorption of dye from aqueous solution by peat, Chem. Eng. J. 70 (1998) 115–124.